Chapter 5

Realization of neutral white light emission in $CaMoO_4$:4%Dy^{3+} phosphor via Sm^{3+} co-doping

"Chapter 5 discusses the study of energy transfer dynamics in Sm^{3+}/Dy^{3+} co-doped $CaMoO_4$ phosphors for single component white light emitters. The chapter deals with the conversion of cold white light to neutral white light by precisely controlling the Sm^{3+} dopant concentration, which is a major drawback for commercial wLEDs. The chapter deals with the study of crystalline structure, particle shape, and size through structural and morphological analysis. The energy transfer process between Dy^{3+} ions and Sm^{3+} ions from the host as well as from Dy^{3+} ion to Sm^{3+} ion is discussed. In the PL decay lifetime section of this chapter, the energy transfer between Dy^{3+} to Sm^{3+} is explained in detail and the energy transfer efficiency is also determined."

5.1 Introduction

In the last decade, white light-emitting diodes (wLEDs) have been preferred over conventional light sources owing to their environmental amiableness, enhanced optical power, and electrical power-saving capacity.[115,169] Most commercial wLEDs nowadays use Ce^{3+}:YAG as the yellow phosphor deposited on the InGaN blue chip to produce white light.[66,67,170] The white light generated by such a device constitutes cold-white light with high correlated color temperature (over 5000 K) due to the lack of red color components[171], taking into account that, we have developed better red and green phosphors have been developed in Chapters 3 and 4. Some researchers have proposed new wLEDs that emit white light using an ultraviolet (UV) LED chip and tri-color (RGB) phosphors. However, this technique has many drawbacks in terms of color ratio adjustment, re-absorption of color, and radiant efficiency.[172,173] Hence, a single-color ingredient phosphor is desired that emits good white light near UV absorption.

Scientists have studied various phosphors as host matrix for developing white-light-emitting phosphors. Many studied phosphors such as $Ba_2Ca(BO_3)_2$, CaF_2, $SrWO_4$, $CaSrAl_2SiO_7$,[118,120,121,174] have various disadvantages such as complex synthesis process which imposes limitations on their large-scale production, low thermal and chemical stability. Therefore, the search to develop chemically and thermally stable phosphors which can be developed by cost-efficient and environmentally friendly technique have gained importance. The molybdates such as $CaMoO_4$ have attracted the interest of the research fraternity owing to their extraordinary qualities. The $CaMoO_4$ has a tetragonal crystal structure with space group $I4_1/a$. $CaMoO_4$ is a self-activated phosphor that emits broadband emission from blue to the yellow visible region centered at a green light when exposed to near UV radiation.[105] In recent years, $CaMoO_4$ is being investigated as a viable phosphor

because of its prominent applications in different fields, such as photoluminescence[45], photocatalysis[12], white light-emitting diodes[24], optical fibers[175], scintillators[176], biomedical applications[74], and laser[177], etc. The advantage of $CaMoO_4$ over other phosphors is that $CaMoO_4$ is thermally and chemically stable and has a stable tetragonal crystal structure. Other advantages of $CaMoO_4$ include a high melting point (1435-1480 ^oC), average effective decay time (14 ms), and non-hygroscopic.[89] The $CaMoO_4$ phosphor is synthesized via different synthesis processes, such as hydrothermal/solvothermal, sol-gel, solid-state technique, and one-step spray pyrolysis.[22,75,77,78,124] Among various synthesis processes, the urea-based auto-combustion process is advantageous over others owing to its cost-effectiveness.

The emitting color can be tuned via doping of various rare-earth elements in $CaMoO_4$ phosphor because of the various arrangements of the 4f electrons. The rare-earth elements have discrete energy levels because of the various arrangement of the 4f electrons. Due to transitions of the 4f electrons among the different energy levels, a variety of fluorescence spectra can be realized. Therefore, most of the rare-earth-doped phosphors have been utilized for various applications[178,179]. The Dy^{3+} doped $CaMoO_4$ phosphor has two intense emission peaks that are observed at 488 nm and 574 nm, which corresponds to the $^4F_{9/2} \rightarrow {}^6H_{15/2}$ and $^4F_{9/2} \rightarrow {}^6H_{13/2}$ transitions of the Dy^{3+} ions, respectively.[24] Under the $CaMoO_4$ excitation, emission spectra of Dy^{3+} doped $CaMoO_4$ illustrate that energy transfer successfully occurs between $[MoO_4]^{-2}$ to Dy^{3+} energy level. Therefore, Dy^{3+} doped $CaMoO_4$ has been used in various applications. The efficiency of both Dy^{3+} emission peaks has a significant impact on the device efficiency of these materials. The overall white emission can be realized by adjusting the intensity of blue and yellow emission of Dy^{3+} ion, but such white light lacks a red component. Earlier reported Dy^{3+} doped phosphors such as

$CaMoO_4$:Dy^{3+}, $Na_3MgZr(PO_4)_3$:Dy^{3+}, $Ba_3La(PO_4)_3$:Dy^{3+}, and $Ba_3Y(PO_4)_3$:Dy^{3+} have studied the luminescence property of Dy^{3+} ion.[24,180–182] The lack of the red component in the overall emission of the Dy^{3+} doped phosphors limits their use in commercial wLEDs. Recently, there are some reports on Dy^{3+}/Sm^{3+} co-doping in other host materials such as $Na_5Y_9F_{32}$, BaY_2ZnO_5, and $Ca_2La_8(SiO_4)_6O_2$ for developing a white light source. But these phosphors have various drawbacks such as the use of the high-temperature solid-state method, and weak self-luminescence[156,183,184].

In this chapter, we have co-doped red-emitting Sm^{3+} ions in 4%Dy^{3+} doped $CaMoO_4$ phosphor for removing the earlier discussed drawbacks as they have a forceful red emission peak at 647 nm ($^4G_{5/2} \rightarrow {}^6H_{9/2}$). The red emission of Sm^{3+} ions in the $CaMoO_4$:4Dy^{3+} shifts the overall emission of Dy^{3+} doped $CaMoO_4$ phosphor from bluish white light to neutral white light. The calculated CCT decreases continuously with Sm^{3+} co-doping in $CaMoO_4$:4%Dy^{3+}. Thus, by adjusting the concentration of the Dy^{3+} and Sm^{3+} ions in $CaMoO_4$, we can achieve excellent white light emissions with CCT < 5000 K. The prepared Sm^{3+}/Dy^{3+} co-doped $CaMoO_4$ phosphors might be used as white light-emitting diode devices.

All the phosphors developed in this chapter are prepared by the urea-assisted internal combustion process, which has been described in detail in Chapter 2, in addition, all the characterization techniques and their models used in this chapter have been described in Chapter 2.

5.2 Results and discussion

5.2.1 XRD analysis

The Rietveld refined XRD pattern of CMO, D4, and S3 has been demonstrated in Fig. 5.1. The XRD pattern corroborates the tetragonal crystal structure of all the prepared phosphors. Some of the observed diffraction peaks such as (101), (112), (004), (200), (212), (204), (220), (116), (312), (224) have been indexed with space group symmetry $I4_1/a$ (JCPDS file number 85-1267 (a=b=5.223, c=11.429))[45]. The structure of $CaMoO_4$ is a 3D framework formed by dodecahedral [CaO_8] clouds and tetrahedral [MoO_4] clouds attached via common vertices Ca–O–Mo.[19] The crystal structure of the prepared phosphor is depicted in Fig. 5.1(d). The ionic radius of Dy^{3+} (91.2 pm) and Sm^{3+} (108 pm) ions are closer to the ionic radius of Ca^{2+} ion (100 pm)[87]. Therefore, it is expected that Dy^{3+} and Sm^{3+} ions must have been substituted in the Ca^{2+} ion sites. The volume of the unit cell and the lattice parameters of all the prepared samples have been obtained by Rietveld refinement using FULLPROF software[85]. The obtained lattice parameters and cell volume of prepared phosphors are shown in Fig. 5.2(a) and tabulated in Table 5.1. For the host phosphor CMO, the cell volume is 312.315 $Å^3$, and the lattice parameters are a=b=5.226 Å, c=11.435 Å, as listed in Table 5.1. The unit cell volume decreases after Dy^{3+} doping in CMO because the ionic radius of the Dy^{3+} ion (102 pm) is less than that of the Ca^{2+} ion (112 pm), the variation in unit cell volume again confirms that Dy^{3+} ions are substituted in Ca^{2+} ion sites. The lattice parameter and the unit cell volume increase with the increasing co-doping concentration of Sm^{3+} because the ionic radii of Sm^{3+} ion (108 pm) is higher than the Dy^{3+} ion and close to Ca^{2+} ion. We have observed that the unit cell volume for a low concentration of Sm^{3+} (for S1 sample) is less than D4 phosphor, which may be due to increased diffusion and migration between different ions. After further increasing the

concentration of Sm^{3+} ion, it occupies the substitutional position, causing an increase in the volume of the unit cell and corresponding transformations in lattice parameters.

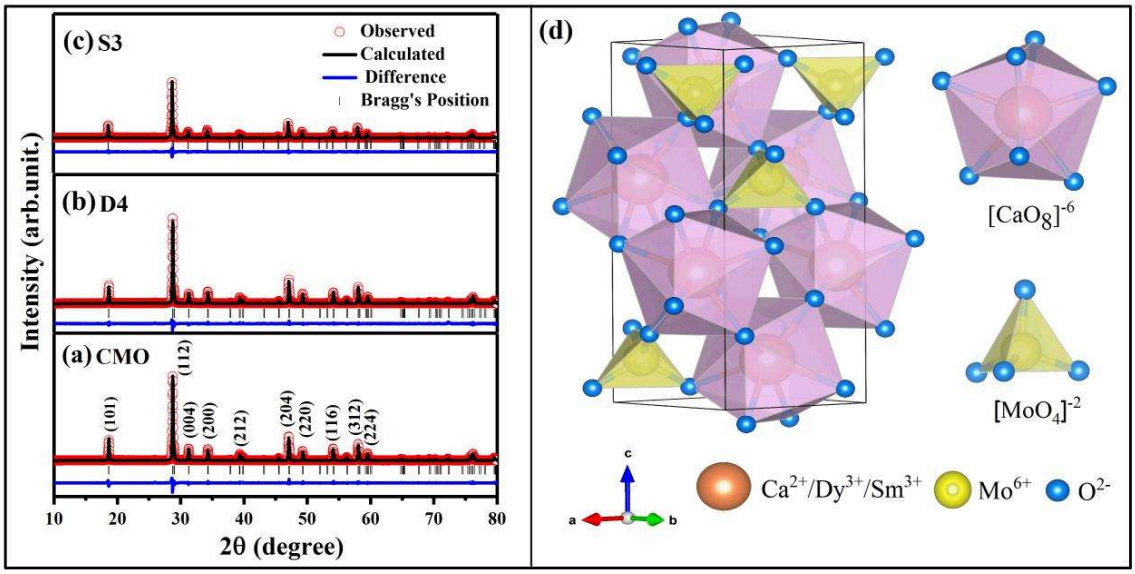

Fig. 5.1 Rietveld refined the XRD pattern of **(a)** CMO, **(b)** D4, **(c)** S3, and **(d)** crystal structure of the S3 sample**.**

We used the Williamson-Hall (W–H) method with the following formula for the calculation of crystallite size (d) and micro strain ($\boldsymbol{\varepsilon}$) in the lattice[88];

$$\beta cos\theta = 4\varepsilon sin\theta + \left(\frac{K\lambda}{d}\right) \qquad 5.1$$

where β is the calculated full width at half maxima (FWHM in radians) computed by deducting instrumental peak broadening ($\beta_{instrument}$) corresponding to the diffraction peak angle θ in the XRD pattern, λ = 1.54 Å is the wavelength of X-ray corresponding to Cu-Kα radiation used in the XRD, and K is a shape factor (K~0.9). The graph of the W-H expression demonstrates a linear equation $y = mx + c$ in the plot of $\beta cos\theta$ versus $sin\theta$. The slope of this linear equation gives the calculated value of the lattice strain (ε), and the intercept of this linear equation gives the crystallite size (d) of the samples. The variation

in crystallite size and lattice strain is shown in Fig. 5.2(b) and is tabulated in Table 5.1. For the $CaMoO_4$ phosphor, the crystallite size is 69 nm, and the microstrain is 0.0028. For Dy^{3+} doped samples, the crystallite size increases, as shown in Fig. 5.2(b). The increased crystallite size indicates more crystallinity of the sample. The 4% Dy^{3+} doped $CaMoO_4$ sample has the maximum crystallite size (76 nm), which illustrates the high crystalline nature of the D4 sample. The crystallite size decreases upon co-doping of Sm^{3+} in $CaMoO_4$:4%Dy^{3+}, as shown in Fig. 5.2(b), but with a further increase in the concentration of Sm^{3+} ion, the crystallite size increases and is maximum (64 nm) for the S3 sample. The increase in the crystallinity of the phosphors results in reducing the density of the grain boundaries. The decrease in grain boundaries helps in improving the luminescence of the phosphor as grain boundaries result in light absorption with is produced within the crystal lattice.[139]

The lattice strain is a measure of the lattice distortions present in the crystal, which arises due to crystal defects. The calculated value of lattice strain for $CaMoO_4$ phosphor is 0.0028 and it reduces with increasing the Dy^{3+} doping percentage. After Sm^{3+} co-doping, the lattice strain is further reduced. The lattice strain remains almost the same as the doping concentration of Sm^{3+} is increased, as presented in the inset of Fig. 5.2(b). The reduced lattice strain indicates that crystal defects decrease in the sample, which helps in emission intensity enhancement.[185]

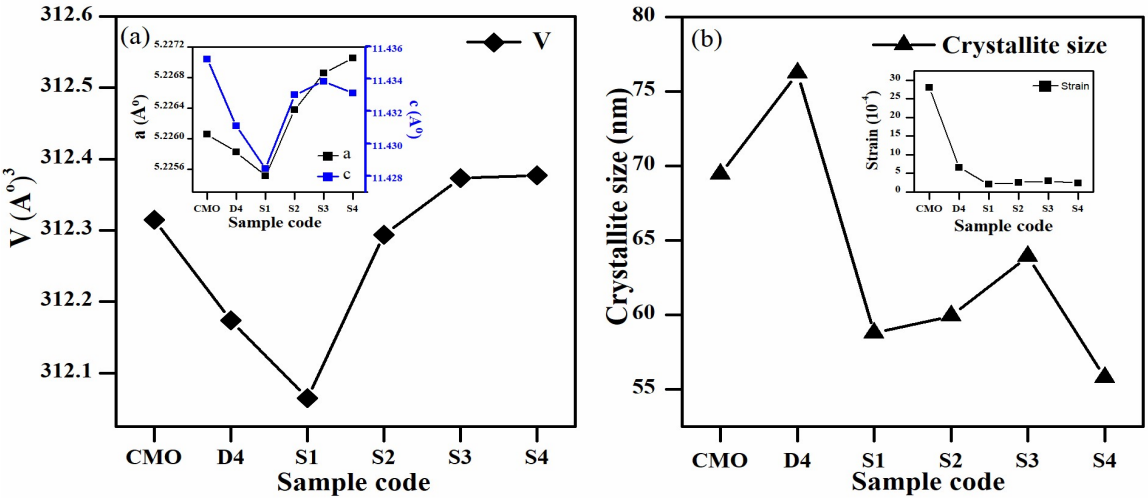

Fig. 5.2 (a) Variation in unit cell volume and lattice parameters (inset) with Sm^{3+} co-doping and **(b)** Variation in crystallite size and lattice strain (inset) with Sm^{3+} co-doping.

Table 5.1 Structural parameters obtained from Rietveld refinement XRD patterns.

Parameters	CMO	D4	S3
Ca (x, y, z) Mo (x, y, z) O (x, y, z)	(0, 1/4, 5/8) (0, ¼, 1/8) (0.1480, 0.0004, 0.2086)	(0, 1/4, 5/8) (0, ¼, 1/8) (0.1479, -0.0016, 0.2093)	(0, 1/4, 5/8) (0, ¼, 1/8) (0.1474, -0.0008, 0.2088)
a=b, c (in Å)	a= 5.2260, c= 11.4352	a= 5.2258, c= 11.4310	a= 5.2268, c= 11.4331
V (in $Å^3$)	312.3148	312.1690	312.3458
χ^2	3.3	2.9	4.5
Crystallite size (in nm)	69.43	76.23	63.90
Microstrain (10^{-4})	28	6.63	3.05

5.2.2 SEM images analysis

The SEM images of CMO, D4, and S3 samples calcined at 1000°C are depicted in Fig. 5.3. The SEM images show the agglomerated spherical shape of particles for CMO, D4, and S3 samples. The average particle size of CMO phosphor is 0.97 µm. Agglomeration

of particles occurs due to the creation of covalent or metallic bonds, which are affected by doping elements. The average particle size increases after Dy^{3+}/Sm^{3+} doping, and the value of average particle size for D4 and S3 samples are 1.21 µm and 1.12 µm, respectively.

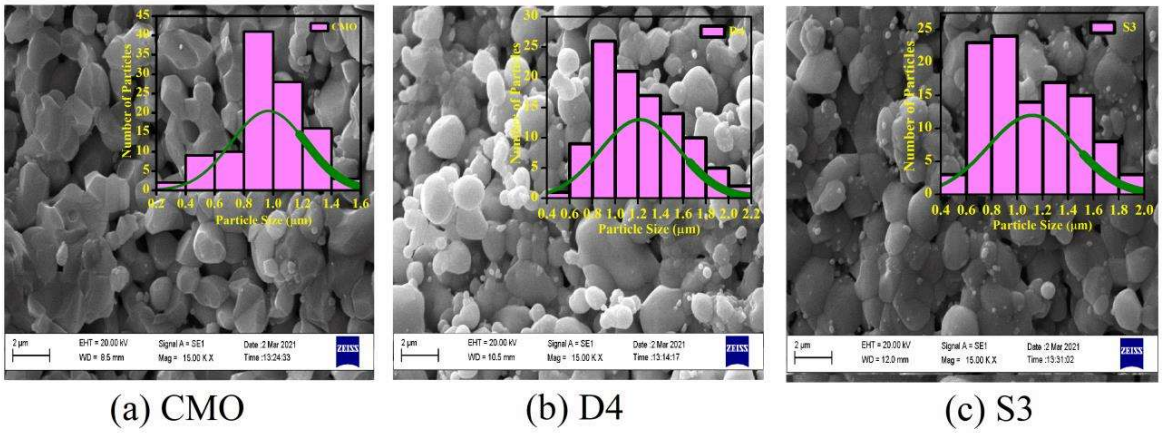

Fig. 5.3 SEM images of **(a)** CMO, **(b)** D4, and **(c)** S3 samples.

5.2.3 XPS analysis

The oxidation states of elements present in the S3 phosphor have been investigated via the XPS technique. The survey scan of S3 is depicted in Fig. 5.4(a). The significant peaks of calcium, molybdenum, oxygen, dysprosium, and samarium are explicitly visible and labeled in the survey scan. The XPS binding energy spectrum of Ca2p, Mo3d, O1s, Dy3d, and Sm3d positions for the S3 sample are shown in Fig. 5.4(b) to 5.4(f). Fig. 5.4(b) shows two bands centered at ~347.28 eV and ~350.78 eV, which are ascribed to $2p_{3/2}$ and $2p_{1/2}$ bound states of Ca^{2+} ion, respectively.[91,92] The XPS spectra of Ca^{2+} ions confirm the +2 oxidation state of calcium in the S3 phosphor. Fig. 5.4(c) shows an XPS scan for the Mo3d core level and the observed peaks are at ~232.88 eV and ~235.98 eV attributed to the binding energy of Mo^{6+} $3d_{5/2}$ and Mo^{6+} $3d_{3/2}$, respectively[91,92], which manifests +6 oxidation state of molybdenum in the S3. Fig. 5.4(d) shows an asymmetric nature in the

XPS scan for the O1s level, which decomposes into two symmetric peaks centered at ~530 eV and ~531.08 eV [53, 54]. This deconvolution of peaks arises from the bonding of oxygen with different elements in the S3 phosphor. The variation in the height of the O1s peak is due to the different electronegativity of the elements present in the sample.[186] The XPS scans of Dy^{3+} and Sm^{3+} ions are presented in Fig. 5.4(e) and Fig. 5.4(f), respectively. The two prominent bands are observed in Fig. 5.4(e), one of them is the asymmetric band that corresponds to the binding energy of Dy3d $3d_{5/2}$, which deconvolute into two symmetrical peaks centered at ~1295 eV, and ~1297.08 eV. The deconvolution of the peaks may be due to spin-orbit splitting in the Dy3d core level.[187,188] The second band centered at ~1334.58 eV is symmetrical, which correlates to the binding energy of $3d_{3/2}$ of Dy3d.[187,188] Fig. 5.4(f) depicts the XPS scan of Sm3d core level with two bands centered at ~1083.08 eV and ~1110.28 eV which are attributed to Sm3d $3d_{5/2}$ and Sm3d $3d_{3/2}$, respectively.[189] The XPS scans manifest that dysprosium and samarium ions are in a +3 oxidation state.

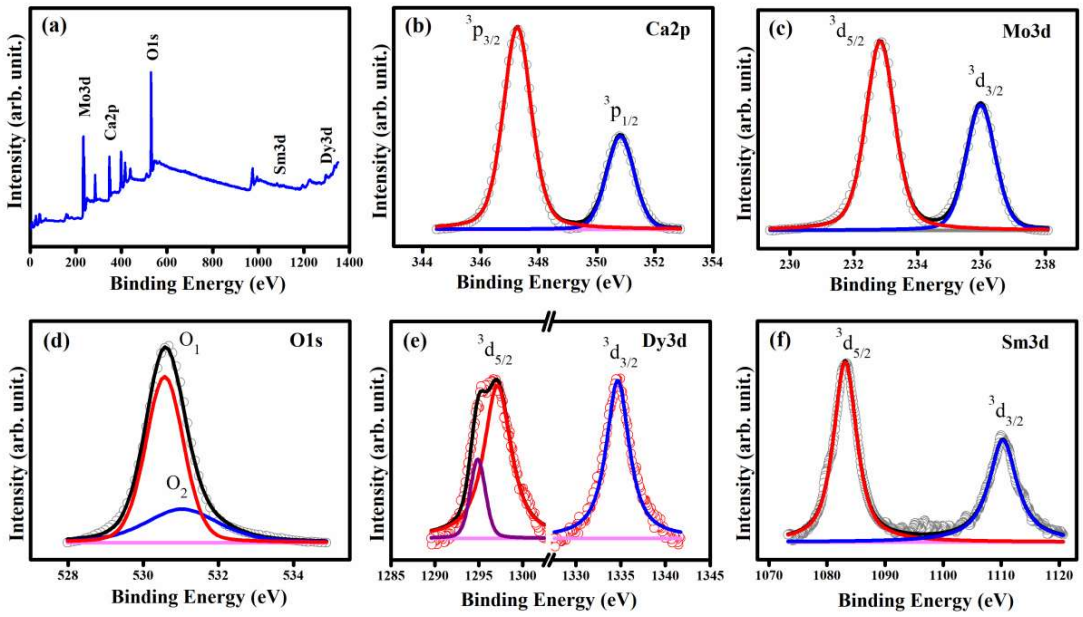

Fig. 5.4 (a) High-resolution XPS survey, XPS spectra of **(b)** Ca2p, **(c)** Mo3d, **(d)** O1s, **(e)** Dy3d, and **(f)** Sm3d for S3 sample.

5.2.4 FTIR analysis

The FTIR spectra of CMO, D4, and S3 samples have been recorded within the wave number range of 400 cm^{-1} to 4000 cm^{-1}. A total of 26 vibrational modes are present in the $CaMoO_4$ crystal structure, which is expressed by the following equation[96],

$$\Gamma = 3A_g + 5A_u + 5B_g + 3B_u + 5E_g + 5E_u \qquad 5.2$$

Out of 26 vibration modes, 8 modes ($4A_u$ + $4E_u$) are infrared active and 13 modes ($3A_g$ + $5B_g$ + $5E_g$) are Raman active. The observed FTIR vibration modes in CMO, D4, and S3 samples are depicted in Fig. 5.5(a) and are tabulated in Table 5.2. The two transmission depths are detected in the fingerprint region from 400 cm^{-1} to 1400 cm^{-1}. One of them has an intense depth which is centered at ~769.45 cm^{-1} and it corresponds to A_u and E_u modes due to anti-symmetric bond stretching of O—Mo—O of $[MoO_4]^{-2}$ tetrahedron. A second

band is observed at ~429.8 cm^{-1} which corresponds to A_u mode arising due to the bending of the Mo–O bond.[45,91] The observed vibrational bands confirm the tetragonal structure of all samples. An additional peak is detected at ~2360 cm^{-1}, corresponding to the vibration of CO_2 in the atmosphere.[45,91]

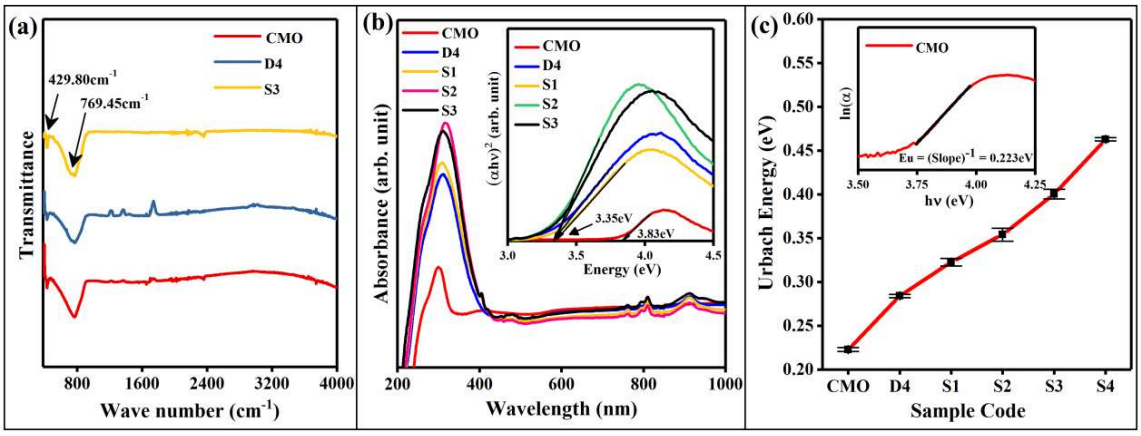

Fig. 5.5 (a) FTIR spectra of CMO, D4, and S3 samples, **(b)** Absorption spectra of Sm^{3+} co-doped phosphors, Inset: Tauc plot for calculating bandgap **(c)** Variation in Urbach energy with Sm^{3+} co-doping. Inset: calculating Urbach energy for CMO sample.

Table 5.2 Obtained vibrational modes of CMO, D4, and S3 samples.

Sample Code	**Vibrational Band** (cm^{-1})		
	Bending of Mo-O bond	**Stretching of O-Mo-O**	**Stretching of O=C=O**
CMO	429.8	769.45	2360
D4	429.8	769.45	2361.2
S3	429.8	769.45	2358.51

5.2.5 Absorption analysis

The absorption spectrums of all phosphors have been recorded in the 200-1000 nm wavelength range. The absorption band obtained for the CMO sample is centered at 300 nm and is shown in Fig. 5.5(b). This absorption band results from charge transfer from O^{2-}

to Mo^{6+}.[190] The absorption band peak shifts at 310 nm after the doping of Dy^{3+}/Sm^{3+} ions. The broadness of the absorption band increases for the Dy^{3+}/Sm^{3+} doped phosphors, which is due to the overlapping of charge transfer bands (CTBs) of O^{2-} to Mo^{6+}, O^{2-} to Dy^{3+} and O^{2-} to Sm^{3+}. Some peaks at 762 nm, 810 nm, and 912 nm are observed in the Dy^{3+} doped $CaMoO_4$ samples, which are ascribed to the transition from $^6H_{15/2}$ to ^6F_J (J=3/2, 5/2, and 7/2) levels of Dy^{3+} ion, respectively. The peaks are in good agreement with the earlier reports.[191] After co-doping of Sm^{3+} ions in the D4 sample, some other peaks are observed at 404 nm and 480 nm which are attributed to $^6H_{5/2} \rightarrow {}^4F_{7/2}$ and $^6H_{5/2} \rightarrow {}^4I_{9/2}$, $^4I_{11/2}$ & $^4I_{13/2}$ transitions of Sm^{3+} ions, respectively.[192]

The optical bandgap (E_g) for prepared samples have been evaluated using the "Wood and Tauc" expression as given below[192];

$$\alpha h\nu = C(h\nu - E_g)^n \qquad 5.3$$

where α is an absorption coefficient, $h\nu$ is the energy of an incident photon, and C is a constant. The nature of the bandgap determines the value of the exponent n. $CaMoO_4$ has an allowed direct bandgap, so the value of n is taken to be 1/2.[145] The intercept of the x-axis of the $(\alpha h\nu)^2$ versus $h\nu$ plot gives the approximate value of the bandgap. The Tauc plot is depicted in the inset of Fig. 5.5(b). The evaluated bandgap of the $CaMoO_4$ is 3.83 eV. The bandgap for Dy^{3+} doped phosphor reduces up to 3.35 eV. The redshift in the bandgap occurs due to the creation of intermediate energy levels of Dy^{3+} in the bandgap.[145] The Sm^{3+} co-doping into 4% Dy^{3+} doped $CaMoO_4$ phosphor does not have much effect on the bandgap.

The Urbach energy (E_u), one of the impacts of structural disorder on the material, gives information on the creation of localized energy levels at the boundary of the energy gap.

The Urbach energy has been calculated for the Sm^{3+} co-doped and Dy^{3+} doped samples via Urbach Empirical formula, as given below expression[147];

$$ln(\alpha) = \left(\frac{h\nu}{E_u}\right) + ln\beta \qquad 5.4$$

where β is a constant, α is the absorption coefficient, $h\nu$ is the photon energy, and E_u represents the calculated Urbach energy. For all the prepared samples, the inverse of the slope of $ln(\alpha)$ versus $h\nu$ plot gives the estimated Urbach energy (E_u), shown in Fig. 5.5(c). The $CaMoO_4$ has the minimum Urbach energy. After that, Urbach energy increases with Dy^{3+} ion doping and also after Sm^{3+} ion co-doping concentration. The decrease in E_u indicates that the defect levels are created in the energy gap. A similar tread in E_u for Dy^{3+}/Sm^{3+} doped phosphor is reported by Halimah *et al.*[193] These defect levels depend on the concentration of dopant ions. It is responsible for the increase in the luminescence intensity by doping of activator ions.[194]

5.2.6 Photoluminescence analysis

5.2.6.1 Excitation (PLE) spectra

The comparative PLE spectrum of CMO, D2, D3, D4, and D5 are presented in Fig. 5.6(a), PLE spectrum of Sm2, Sm3, and Sm4 in Fig. 5.6(b), and the PLE spectrum of D4, S1, S2, S3, and S4 in Fig. 5.6(c). The PLE spectra of CMO are obtained for 500 nm emission wavelength. The broadband in the PLE spectrum of CMO centered at 296 nm is accredited to the ligands to metal charge transfer (LMCT) band, which is the result of charge transfer from the filled 2p orbital of O^{2-} ion to the partially filled orbital of Mo^{6+} ion within the $[MoO4]^{-2}$ groups. The PLE spectra of the Sm series are obtained by monitoring $^4G_{5/2} \rightarrow {}^6H_{9/2}$ (646 nm) Sm^{3+} emission transition. The broadband shown in Fig. 5.6(b) is attributed to the overlap of the LMCT band and charge transfer band (CTB). It is observed that for

higher Sm^{3+} doping in $CaMoO_4$, the intensity of the broadband is increased and the broadband is also shifted to the higher wavelength. The shift and increase in the broadband are attributed to the overlap of the LMCT and CTB bands. Some f—f transitions of Sm^{3+} ion are also visible in the PLE spectrum, which is attributed to the energy transfer from the ground level $^6H_{5/2}$ to higher levels $^4L_{17/2}$ (367 nm), $^4K_{11/2}$ (378 nm), $^4F_{7/2}$ (407 nm), $^6P_{5/2}$ (422 nm), $^4I_{13/2,\ 11/2,\ 9/2}$ (465—483 nm).[143] The PLE spectrum of the D and S series was obtained by monitoring $^4F_{9/2} \rightarrow {}^5H_{13/2}$ (574 nm) Dy^{3+} emission transition. The broadband of excitation spectra centered at 296 nm have been recorded from 230 nm to 340 nm, which is attributed to the overlap of the LMCT band and CTB.[23] The CTB is due to charge transfer from the filled 2p orbital of the O^{2-} ion to the partially filled orbital of Dy^{3+} and Sm^{3+} ions. Some f—f transitions of Dy^{3+} ion are also visible in the PLE spectrum, which is attributed to the energy transfer from the ground level $^6H_{15/2}$ to higher levels $^6P_{3/2}$ (327 nm), $^6P_{7/2}$ (352 nm), $^6P_{5/2}$ (366 nm), $^4I_{13/2}$ (388 nm), $^4G_{11/2}$ (427 nm), $^4I_{15/2}$ (453 nm), and $^4F_{9/2}$ (476 nm). All observed excitation peaks of Dy^{3+}ion are in good agreement with the earlier reports.[195]

The PLE intensity is increased by increasing the doping percentage of Dy^{3+} ions, and consequently, D4 records the maximum intensity. After that, quenching is observed in the excitation spectrum, as shown in Fig. 5.6(a). The intensity of the excitation peaks corresponding to Dy^{3+} ion decreases with an increase in the co-doping percentage of Sm^{3+} ions in the D4 sample. The decrease in the excitation intensity is the result of energy transfer from Dy^{3+} ions to Sm^{3+} ions.

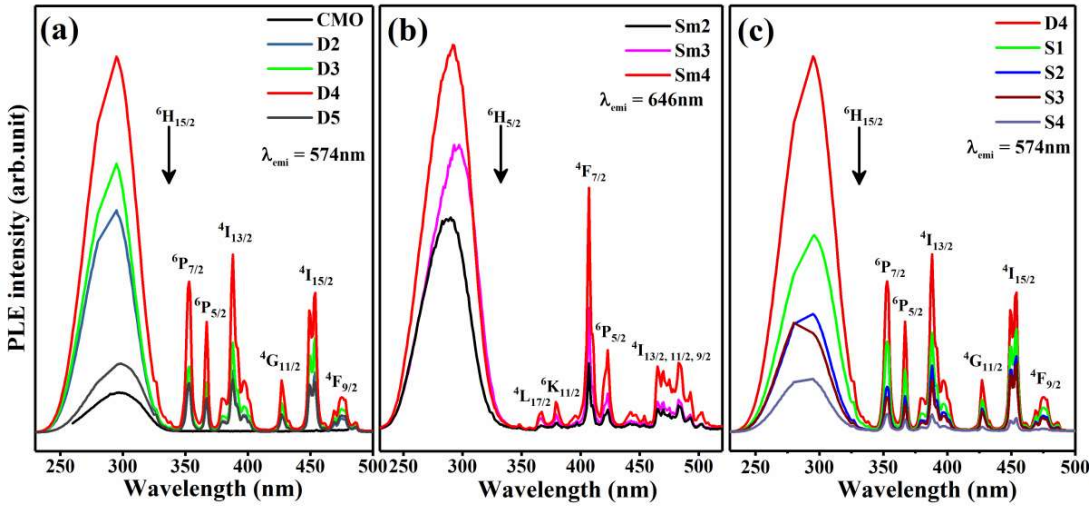

Fig. 5.6 PL excitation spectra for **(a)** Dy^{3+} doped phosphors, **(b)** Sm^{3+} doped phosphors, and **(c)** Sm^{3+} co-doped CaMoO4:4%Dy^{3+} phosphors.

5.2.6.2 Emission (PL) spectra

The comparative PL spectra of CMO, D2, D3, D4, and D5 are depicted in Fig. 5.7(a), the PL spectra of Sm2, Sm3, and Sm4 in Fig. 5.7(b), and the PL spectra of D4, S1, S2, S3, and S4 in Fig. 5.7(c). The broadband in the PL spectra of CMO is centered at 500 nm which is because of the energy transfer from the conduction to the valance band.[23] A variation in the intensity of broadband emission has been observed for Dy^{3+} doped phosphors, which indicates the effective charge transfer from CMO to Dy^{3+} ions. The broadband emission intensity is lowest for the D4 concentration, as shown in Fig. 5.7(a). Some sharp peaks corresponding to Dy^{3+} transitions are observed at 488 nm ($^4F_{9/2} \rightarrow {}^6H_{15/2}$) and 574 nm ($^4F_{9/2} \rightarrow {}^6H_{13/2}$).[196] The $^4F_{9/2} \rightarrow {}^6H_{15/2}$ transition is the magnetic dipole transition, while the $^4F_{9/2} \rightarrow {}^6H_{13/2}$ transition is the electric dipole transition of Dy^{3+} ions, which is allowed at lower symmetries without an inversion center.[196] The chemical environment of Dy^{3+} ions realty affects the electric dipole transition, whereas the magnetic dipole transition is less sensitive to the chemical environment. Therefore, yellow emission (574 nm) is much more intense

compared to blue emission (488 nm) as shown in Fig. 5.7(a). The radius of the Dy^{3+} ion is comparable to the radius of the Ca^{2+} ion, so Dy^{3+} ions can enter into low symmetry Ca^{2+} sites without an inversion center. Hence, we observe strong $^4F_{9/2} \rightarrow {}^6H_{13/2}$ electric dipole transition for Dy^{3+} doped phosphors. A weak band is also observed in the red region at 661 nm, which is due to the $^4F_{9/2} \rightarrow {}^6H_{11/2}$ transition. Some transition peaks are split into two or three emission peaks, which is due to the crystal field effect.[197] All emission transitions of Dy^{3+} ions are in good agreement with earlier reports.[195] Variation in 574 nm peak intensity with the Dy^{3+} doping concentration is plotted in the inset of Fig. 5.7(a). The PL intensity increases with increasing the doping percentage of Dy^{3+} and the maximum emission is observed D4 sample. After 4% concentration, we observe a quenching phenomenon which results in a decrease in emission intensity at higher Dy^{3+} concentrations.[107] The PL spectra of the Sm series in Fig. 5.7(b) shows broadband centered at 500 nm which is attributed to the overlap of LMCT and CTB. Some characteristic peaks of Sm^{3+} ions which are attributed to the energy transfer from $^4G_{11/2}$ to lower levels $^6H_{5/2}$ (562 nm), $^6H_{7/2}$ (605 nm), $^6H_{9/2}$ (646 nm) are also observed in Fig. 5.7(b). It is observed that the emission intensity of the broadband decreases while the intensity of characteristic peaks increases, which is attributed to the energy transfer from CMO to Sm^{3+} ions.

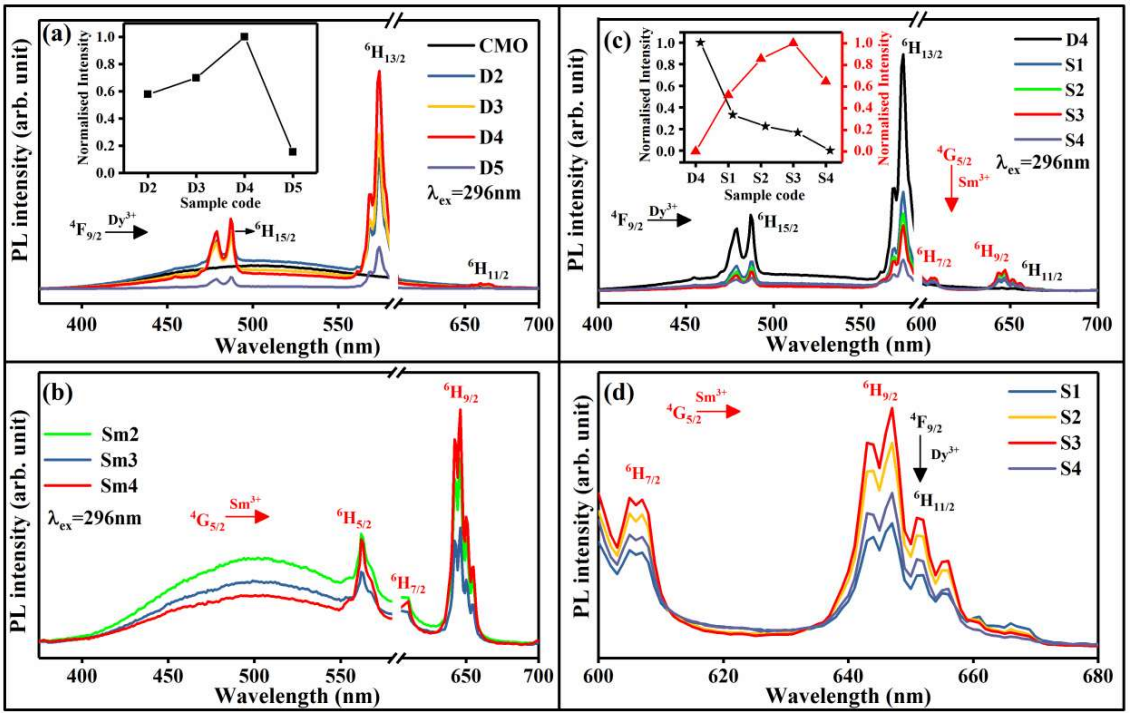

Fig. 5.7 PL emission spectra for **(a)** Dy^{3+} doped phosphors, **(b)** Sm^{3+} doped phosphors, **(c)** Sm^{3+} co-doped $CaMoO_4$:4%Dy^{3+} phosphors, and **(d)** PL emission in the range from 600 nm to 680 nm for Sm^{3+} co-doped $CaMoO_4$:4%Dy^{3+} phosphors.

This relative distance (d_r) between the emitting ions depends upon the critical concentration (c) of the activator ion, the volume of the unit cell (V), and the number of host cations per unit cell (N). And the relative distance (d_r) expression is written as below[152];

$$d_r = 1.24 * \sqrt[3]{\frac{V}{c * N}} \qquad 5.5$$

The unit cell volume (V) of the D4 sample is 312.169 $Å^3$, which is estimated from XRD analysis, critical concentration (c) of Dy^{3+} ion is 0.04, and the number of available lattice sites of $CaMoO_4$ in per unit cell (N) is 4. After calculation, the critical relative distance is 1.55 nm. Generally, quenching occurs either due to energy exchange or due to electrical multipolar transitions. The energy exchange occurs because of the overlap of the Dy^{3+} wave functions and the relative distance between Dy^{3+} ions must be less than 0.5 nm.[198] The

calculated d_r indicates that the non-radiative energy transfer is not due to the overlap of the wave-functions of the Dy^{3+} ions but may be due to the electric multipolar interaction.

The form of multipolar interaction, which is responsible for quenching in $CaMoO_4$: x%Dy^{3+}, can determine by using the theory of Dexter. Dexter's expression can be converted in logarithm form, given by the following equation[153];

$$log\left(\frac{I}{x}\right) = C - \frac{Q}{3}log(x) \qquad 5.6$$

where C is any constant, x (x= 2%, 3%, 4%, and 5%) is the percentage of Dy^{3+} doping concentration, and I denotes the intensity of transition peak correlated to Dy^{3+} doping percentage. The Q value gives information on multipolar interaction, Q value represents dipole-dipole interaction, dipole-quadrupole interaction, and quadrupole-quadrupole interaction according to Q = 6, 8, and 10, respectively. The value of Q for 574 nm corresponding to Dy^{3+} emission transition $^4F_{9/2} \rightarrow {}^6H_{13/2}$ is thrice the negative slope of the plot *log(I/x)* versus *log(x)*. The *log(I/x)* versus *log(x)* plot is depicted in Fig. 5.8. The value of Q for the yellow emission peak is 5.92, near around 6. Hence, the multipolar interaction is dipole-dipole interaction in Dy^{3+} doped $CaMoO_4$.

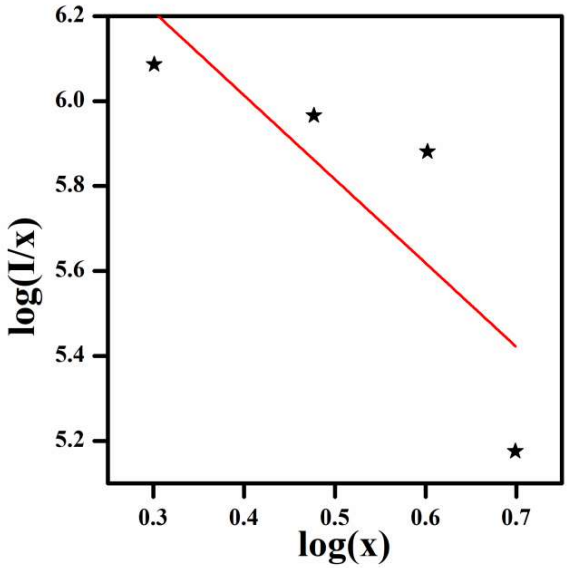

Fig. 5.8 log (I/x) versus log(x) plot for calculating multipolar interaction.

The energy transfer from Dy^{3+} to Sm^{3+} is realized by co-doping Sm^{3+} in the D4 phosphor. The PL spectra of Sm^{3+} co-doped $CaMoO_4$:4Dy^{3+} phosphors are presented in Fig. 5.7(c). Some other emission peaks around 605 nm and 646 nm are observed which corresponds to the Sm^{3+} transition from $^4G_{5/2}$ to ^6H_j (j = 7/2, 9/2), respectively. The Sm^{3+} ion transition $^4G_{5/2} \rightarrow {}^6H_{7/2}$ (orange emission at 605 nm) is the magnetic dipole transition, and the $^4G_{5/2} \rightarrow {}^6H_{9/2}$ transition (red emission at 647 nm) is the forced electric dipole transition.[72] The ionic radius of Sm^{3+} (108 pm) is comparable to the ionic radius of Ca^{2+} ion (112 pm), so the Sm^{3+} ions are placed easily in low symmetric sites of Ca^{2+} ions without an inversion symmetry similar to Dy^{3+} ions. All transition peaks of Sm^{3+} are in good agreement with the earlier reports[143]. The splitting of transition peaks occurs due to the crystal field effect. From Fig. 5.7(c & d), we infer that the emission intensity of the broadband and peaks corresponding to Dy^{3+} transition decreases, while the intensity of peaks corresponding to Sm^{3+} ions increases with the increase in the co-doping concentration of Sm^{3+} ions. This

variation in the intensities of the broadband and emission peaks corresponding to CMO, Dy^{3+} and Sm^{3+} ions manifests that energy transfer occurs from the CMO and Dy^{3+} ions to Sm^{3+} ions. The energy transfer occurs from the conduction band of $CaMoO_4$ to the intermediate excited levels of the Dy^{3+} and Sm^{3+} ions. Further, since the $^4G_{5/2}$ transition level of Sm^{3+} ions lies below Dy^{3+} transition levels, therefore energy transfer from Dy^{3+} to Sm^{3+} energy levels is prompted. The schematic of energy transfer process from the host to Dy^{3+}/Sm^{3+} ions and Dy^{3+} to Sm^{3+} energy levels is shown in the energy level diagram in Fig. 5.9(a). It is observed that the 3% Sm^{3+} co-doped phosphor has the maximum emission intensity, Fig 5.7(c) and 5.7(d). On further increasing the doping percentage of Sm^{3+}, the intensity of Sm^{3+} emission transitions is quenched. The intensity variation of the strong emission of Dy^{3+} and Sm^{3+} ions in the Sm^{3+} co-doped D4 samples is shown in the inset of Fig. 5.7(c). Thus, energy is easily transferred from the host energy band to the Dy^{3+}/Sm^{3+} energy levels and from the Dy^{3+} energy levels to the Sm^{3+} energy levels. It is inferred that the Sm^{3+}/Dy^{3+} doped $CaMoO_4$ phosphor can produce white light by regulating the concentration of Dy^{3+} and Sm^{3+} ions. The prepared Sm^{3+}/Dy^{3+} doped $CaMoO_4$ phosphors can be used as a white light-emitting material in various optoelectronic devices, such as wLEDs.

5.2.6.3 PL decay analysis

The normalized PL decay curves of D4 and S3 phosphors in logarithmic scale for $^4F_{9/2} \rightarrow {}^6H_{13/2}$ transition (574 nm) upon 353 nm excitation are depicted in Fig. 5.9(b). We have examined the decay curves by fitting them with the biexponential equation[183];

$$I(t) = I_0 + A_1 \, exp\left(-\frac{t}{\tau_1}\right) + A_2 \, exp\left(-\frac{t}{\tau_2}\right) \qquad 5.7$$

where I_0 is the background intensity at a long time after excitation and I is the intensity after t seconds; fast and slow decay times are denoted by τ_1 and τ_2, respectively; A_1 and A_2 are the fitting constants. To calculate the average lifetime we have used the following relation[183];

$$\tau_{avg} = \frac{A_1\tau_1^2 + A_2\tau_2^2}{A_1\tau_1 + A_2\tau_2} \quad 5.8$$

From equations 5.7 and 5.8, the average lifetime of the $^4F_{9/2}$ level of the Dy^{3+} ion for D4 and S3 is 2.75 ms and 1.37 ms, respectively. It was observed that the lifetime of Dy^{3+} ions is decreased after 3% Sm^{3+} ions co-doping, which indicates the energy transfer process from Dy^{3+} to Sm^{3+} ions. The energy transfer efficiency (η_{ET}) can be calculated using the following relation

$$\eta_{ET} = 1 - \frac{\tau_x}{\tau_0} \quad 5.9$$

where τ_x and τ_0 are the average lifetime of $^4F_{9/2}$ level of the Dy^{3+} ion in S3 and D4 sample, respectively. The calculated η_{ET} is 50.1%, which is higher than many of the earlier reported phosphors with Dy^{3+} and Sm^{3+} co-doping.[183,184] The high value of η_{ET} support our analysis of energy transfer from Dy^{3+} to Sm^{3+} ions which we have discussed in the previous section.

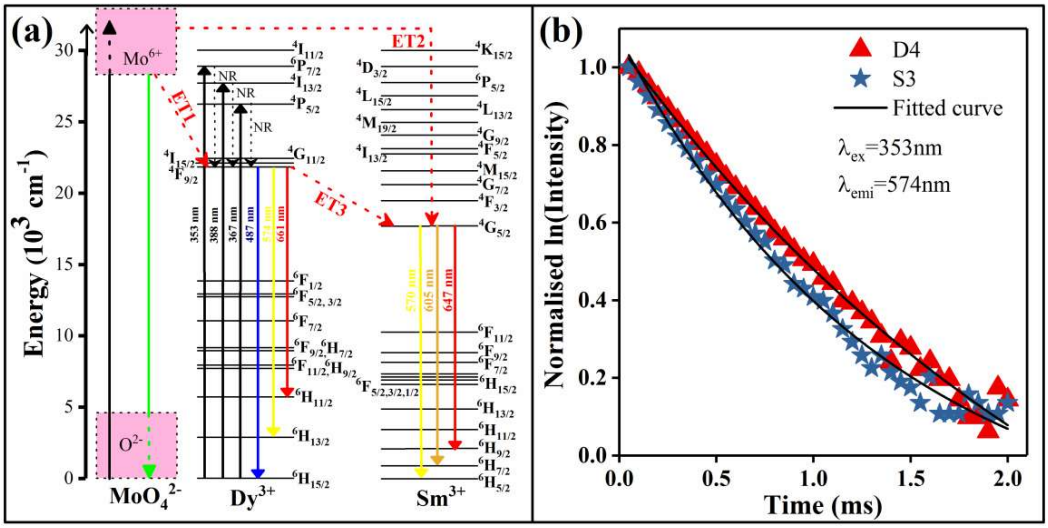

Fig. 5.9 (a) Energy transfer mechanism of $[MoO_4]^{2-}$, Dy^{3+} and Sm^{3+}, **(b)** PL decay curves of D4 and S3 phosphors.

5.2.7 Chromaticity parameters

The Commission Internationale de l'Elcairage (CIE) coordinates of D4, S1, S2, and S3 samples are calculated from their emission spectra and are labeled in the chromaticity diagram shown in Fig. 5.10 and the calculated CIE coordinate is tabulated in Table 5.3. The evaluated CIE coordinates for D4 are (0.3364, 0.3975), which lies in the near-white light region. For Sm^{3+} co-doped phosphor, CIE coordinates shift towards the red color region. The overall emission represents a white color with a combination of Dy^{3+} emission (blue & yellow peaks) and Sm^{3+} emission (red peak).

The correlated color temperature (*CCT*), which determines the calculated color temperature of the prepared phosphors used to concern quality of light can be calculated by using the given below equation[64];

$$CCT = -437n^3 + 3601n^2 - 6861n + 5514.31 \qquad 5.10$$

where $n = \frac{(x-x_e)}{(y-y_e)}$ and the value of coordinate (x_e, y_e) is (0.33, 0.1858). The calculated *CCT* for 4% Dy^{3+} doped $CaMoO_4$ phosphor is 5389 K, which is in the cold white light region (>5000 K). However, the calculated *CCT* of Sm^{3+} co-doped phosphor is 4439 K, which illustrates that emitting light color is moved from cold to neutral white light region. Similar observations have been also reported earlier by A. U. Trápala-Ramírez *et al.*[37] The calculated *CCT* for all samples is listed in Table 5.3. It is inferred that the CIE coordinates and *CCT* value can be altered by regulating the Dy^{3+}/Sm^{3+} doping concentration in the $CaMoO_4$ phosphor.

The color purity which represents the purity of mono chromaticity of the overall emission is tabulated in Table 5.3. It is evaluated by the following expression[37];

$$color\ purity\ (\%) = \frac{\sqrt{(x_s-x_i)^2+(y_s-y_i)^2}}{\sqrt{(x_d-x_i)^2+(x_d-x_i)^2}} * 100 \qquad 5.11$$

where (x_s, y_s) are the coordinates of the prepared phosphor and (x_i, y_i) are the coordinates of the white illumination point (0.3101, 0.3162) of the 1931 CIE Standard Source C. The (x_d, y_d) coordinates lie on the perimeter of the CIE diagram, which can be obtained by expanding the straight line between (x_i, y_i) and (x_s, y_s) up to the perimeter. The lower value of color purity percentage means that the overall emission of the phosphor is closer to white light. The calculated color purity percentage of all Sm^{3+} co-doped $CaMoO_4$:4Dy^{3+} phosphors is in the range of 19%-22% which is low, therefore it suggests that the overall emission of all phosphors is closer to white light.

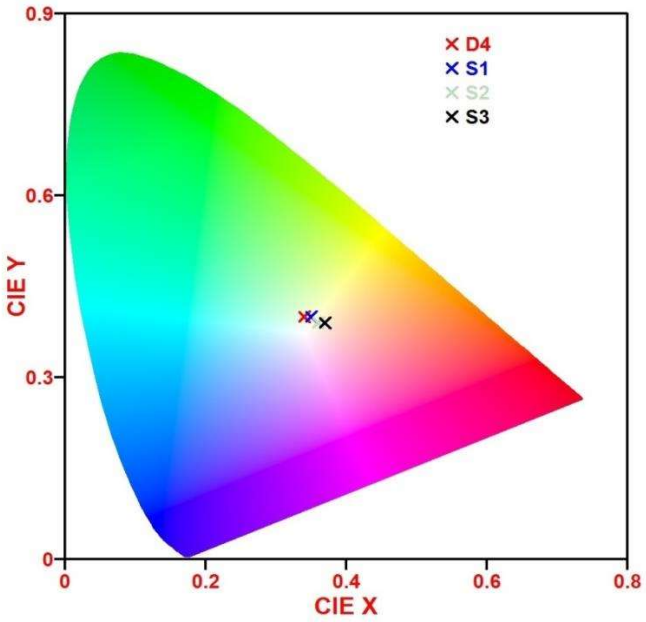

Fig. 5.10 Chromaticity diagram of Sm^{3+} co-doped phosphors.

Table 5.3 Chromaticity parameters of D4, S1, S2, and S3 phosphors.

Sample code	CIE coordinate (x, y)	CCT (K)	Light Color	Color purity (%)
D4	(0.336, 0.397)	5389	Cold white light	19.1
S1	(0.345, 0.392)	5122	Cold white light	20.2
S2	(0.353, 0.387)	4867	Neutral white light	20.9
S3	(0.366, 0.380)	4439	Neutral white light	22.2

5.3 Conclusions

In the present study, we have successfully synthesized $CaMoO_4$, Dy^{3+}/Sm^{3+} doped $CaMoO_4$, and Sm^{3+} co-doped $CaMoO_4$:4Dy^{3+} phosphors via the facile auto-combustion process. The structural analysis confirms the tetragonal crystal structure of $CaMoO_4$ and other doped phosphors. The PL spectrum depicts emission peaks of Dy^{3+} doped $CaMoO_4$ phosphors at 487 nm and 574 nm for near-UV light excitation (296 nm). After 4% Dy^{3+} concentration, quenching in emission intensity is observed which is due to dipole-dipole

interaction between the Dy^{3+} ions in $CaMoO_4$. The shift from bluish-white light to neutral white light is observed when Sm^{3+} ions are co-doped in $CaMoO_4$:4Dy^{3+} phosphor. The shift in the color of overall emission is attributed to the efficient energy transfer process from CMO to Dy^{3+}/Sm^{3+} ions and from Dy^{3+} to Sm^{3+} ions. The process of energy transfer is discussed in detail with the help of an energy level diagram. The average lifetime of the $^4F_{9/2}$ level of the Dy^{3+} ion is decreased with Sm^{3+} ion co-doping. The decreased average lifetime validates energy transfer from Dy^{3+} to Sm^{3+} ions and the calculated energy transfer efficiency is around 50% for the S3 sample. It is observed that the Dy^{3+}/Sm^{3+} co-doped phosphors have low CCT values and low color purity percentages. Thus, the prepared Dy^{3+}/Sm^{3+} co-doped $CaMoO_4$ phosphor can be a good alternative for various optoelectronic applications.